

FIRST PRINCIPLE STUDY OF ELECTRONIC PROPERTIES OF 2D MXene FOR MXene/METAL OXIDES MEMRISTOR APPLICATION

J. WEN^{a,*}, Q. OU^a, B. XIONG^a

School of Information Engineering, Nanchang Hangkong University, 330063, Nanchang, P. R. China

Physical role of a novel two-dimensional (2D) MXene material, Cr₂C, in determining the electrical conduction behavior of metal oxide memristor was studied here. Today one emerging application of 2D MXene materials is possessed from its ability to accelerate the formation of the conductive filaments inside the resistive oxide-based memristor device. The cause of such an improvement however remains mysterious. To address this issue, Cr₂C, was introduced into the Ag/Cr₂C/Pt stack to calculate its electronic structure and conductive characteristics via density functional theory. It was found that that most regions inside the Ag/Cr₂C/Pt stack were occupied by electrons. The studied stack without the presence of an energy gap indicated its metal-like property. Additionally, the investigated Ag/Cr₂C/Pt stack generated lower energy barrier than other conventional MXenes such as Ti₃C₂ and V₂N. Such low energy barrier led to higher device electron diffusivity, mobility, and electrical conductivity. This undoubtedly benefited the formation of the conductive filaments inside the memristor device.

(Received December 21, 2020; Accepted March 16, 2021)

Keywords: MXenes, Cr₂C, Electrical conduction, Memristor, Density-functional theory

1. Introduction

Traditional von Neumann digital computers are being subjected to the severe computational drawbacks due to the separation of data processing from data storage [1-3]. Memristor with a unique function of merging processing and storage modes is thus considered as one of the most promising approaches to overcome von Neumann bottleneck, thereby paving a new route towards brain-inspired computing architecture [4-6]. The brain-like behavior of memristor arises from its exotic resistive switching (RS) phenomenon that can sustain the internal resistance state based on the external electrical excitations. Such RS trait has been commonly found on various binary transition metal oxides such as TiO₂ [7, 8], HfO₂ [9, 10], ZrO₂ [11, 12], TaO₂ [13, 14], and SiO₂ [15, 16], consequently making them suitable for memristor and artificial synapse and neuron applications. Among these materials, SiO₂-based resistive memristor has most recently attained particular interest owing to its excellent scalability, fast switching speed, low energy consumption, and good compatibility with silicon Complementary Metal-Oxide-Semiconductor (CMOS) circuits. However, its RS mechanism still remains controversial, and its future commercial applications on data storage and neuromorphic computing

* Corresponding author: wenj@nchu.edu.cn

is stringently hindered by the reported RS variability [17, 18].

One possible scenario to address above issues is to position a two-dimensional (2D) MXene material between the top electrode and the metal oxides inside the resistive memristor architecture to mitigate its memristive performance [19, 20]. The 2D MXene materials, pioneered by the synthesis of Ti_3C_2 , are derived by exfoliating the so-called MAX phases, and have been shown promising particularly for energy storage applications [21-23]. Owing to its advantageous attributes such as high stacking density, hydrophilicity, and large electrical conductivity, using MXene as a functional layer inside the SiO_2 -based memristor device has recently been proposed, providing a capability of repeatable bipolar RS at low operating voltages, multilevel RS states, and a relatively high retention [24, 25]. These improvements are critical for the future neuromorphic computing, and likely due to the preferential growth of conductive filaments (CF) along the MXene location as well as the reduced randomness of CF across the whole memristor nanostructure [26]. Nevertheless, the key factors responsible for such improvements are rarely studied either by experiments or by simulations up to date. Additionally, MXene material devoted to the memristor applications is currently focused on Ti_3C_2 , while very few study has assessed the role of other promising MXene materials in determining the conductive performances of the memristor device. In contrast to conventional 2D Ti_3C_2 and Ti_3N_2 that exhibit antiferromagnetic characteristics [27], 2D Cr_2C was reported to be ferromagnet that can be exfoliated from their MAX phases [28]. Such magnetic property is usually attributed to the d-orbitals of Cr atoms, and the Cr_2C system can possibly sustain its magnetic trait nearly up to room temperature [29]. Besides above difference, 2D Cr_2C is also stable in MXene phase owing to its larger negative formation enthalpy than conventional MXene materials [30]. It has been therefore considered as a promising Li storage material for lithium ion battery [31]. In spite of its storage function, its electronic property and prospect for the metal oxide application remains un-clear. To deeply understand the function of MXene for the RS mechanism of memristor device, and to explore alternative MXene candidates for the future neuromorphic computing, we developed a sophisticated model based on density functional theory (DFT) to calculate the electronic structure and conductive characteristics of the MXene Cr_2C for a typical memristor structure of Ag/ MXene /Pt.

It should be noted that metal oxide (i.e., memristive media) was not introduced into our current model. This is mainly due to the complex electronic structure of oxygen. Metal oxide generally carries oxygen vacancies or extra oxygen, causing the chemical valence of metal oxides other than an integer. This usually gives rise to a magnetic system with very complex electronic structure that is hard to be simulated. In addition, the presence of oxygen vacancy and extra oxygen can significantly change the system structure that generally is asymmetric and irregular. As a result, the complex extent to the computation was remarkably augmented, making the simulation hard to be converged.

2. Methods

All density functional theory (DFT) calculations involved in this work were conducted by Dmol3 package [32]. The lattice parameters of Cr_2C , Ag and Pt were firstly optimized, and subsequently used to build surfaces and layer structures. Perdew-Burke-Emzerhof (PBE) functional was used in this work [33], and the calculation basis was set to dynamic nuclear spin

polarization (DNP). The cut-off distance and the electron density convergence were set to 4.4 Å and 10^{-4} , respectively. To build a Ag/Cr₂C/Pt hetero-structure, we constructed Cr₂C(001), Ag(111) and Pt(111) surfaces [34]. These surfaces are combined together by depositing Ag(111) at the uppermost layer and Cr₂C(001) at the middle layer and Pt(111) at the bottommost layer, as depicted in Figure. 1(a). Such 3-layer structure was used to make a 4×4 Ag/Cr₂C/Pt supercell, encapsulated by a 25 Å vacuum layer. The k-meshes of the Ag/Cr₂C/Pt structure during all calculations were considered as 4×4×1. To calculate the Ag diffusion across Ag/Cr₂C/Pt structure, an Ag ion was positioned at the top/bottom side of Ag/Cr₂C/Pt structure as the initial/final state (IS/FS) structure, respectively. The transitional state (TS) structure was searched using the linear synchronous transit (LST)/quadratic synchronous transit (QST) scenario [35]. The diffusion barrier E_a was determined using the formula: $E_a = E_{TS} - E_{IS}$, where E_{TS}/E_{IS} indicates the energy of the transitional/initial state structure.

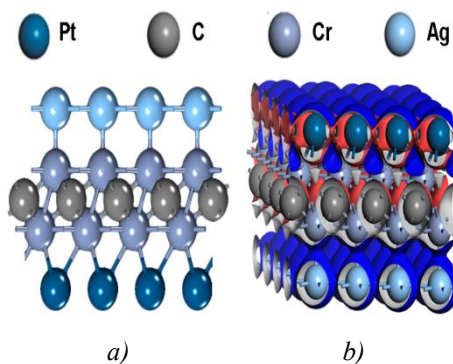


Fig. 1 (a) Geometry and (b) electron density plot of Ag/Cr₂C/Pt structure. For (b), blue and red contours represent the electron accumulation and neutral charge, respectively.

3. Results and discussion

The electron densities of the Ag/Cr₂C/Pt structure, as shown in Fig. 1(b), reveals that most regions are occupied by electron-rich environment, possibly owing to its metal compositions that induce excess electrons. There only exists few electron-loss regions confined at areas near Cr₂C(001) and Pt(111) layers. It is indicated in Figure. 1(b) that the electrons can move freely around the Ag/Cr₂C/Pt structure, leading to a high electrical conductivity. The initial state, transition state and final state of the Ag diffusion process are described in Fig. 2. For the initial state, the diffusive Ag ion is located at the bottom of the slab, i.e. at the Ag(111) surface side. During the diffusion process, this Ag ion penetrates through the Ag(111)-Cr₂C(001)-Pt(111) layers. Along the diffusion path, the state with the highest energy is assigned to be the transition state, in which the Ag ion is inside the Cr₂C(001) layer. After passing through the Cr₂C(001) layer, the system energy decreases and the Ag ion finally reaches the diffusion termination at Pt(111) side.

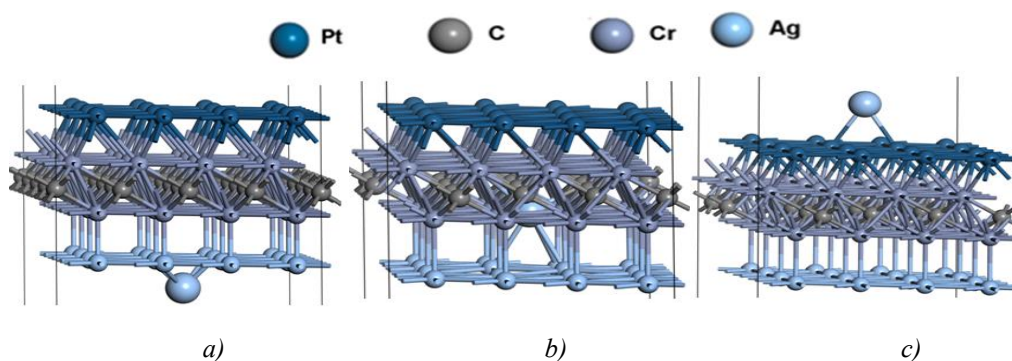


Fig. 2 Ag diffusion through the Ag/Cr₂C/Pt stack in its (a) initial state, (b) transition state, and (c) final state. The diffusive Ag ion is highlighted with larger radius than other atoms.

The highest occupied molecular orbital (HOMO) and lowest unoccupied molecular orbital (LUMO) structures of Cr₂C media were also calculated and illustrated in Fig. 2. It is observed from Fig. 2(a) that most HOMO are located around the Cr atom rather than C atom, which likely indicates that the Cr atom possesses higher activity than C atom. Moreover, the side views of HOMO also show strong bonding between Cr-Cr by d orbital at the surface regions, suggesting a good surface reactivity from Cr component. However, there are few HOMO region around C atoms, meaning the inertness in interior regions of Cr₂C. With regards to the LUMO structure (Fig. 2(b)), most yellow and cyan regions are distributed periodically along the same direction. For example, the yellow regions cover some surface C atoms and interior Cr atoms that are not directly bonded with each other, whereas the cyan regions cover surface Cr atoms and interior C atoms that also are not directly connected. These results imply that the LUMO structure reflects no bonding information of Cr₂C structure, which in turn demonstrates the stability of Cr₂C structure.

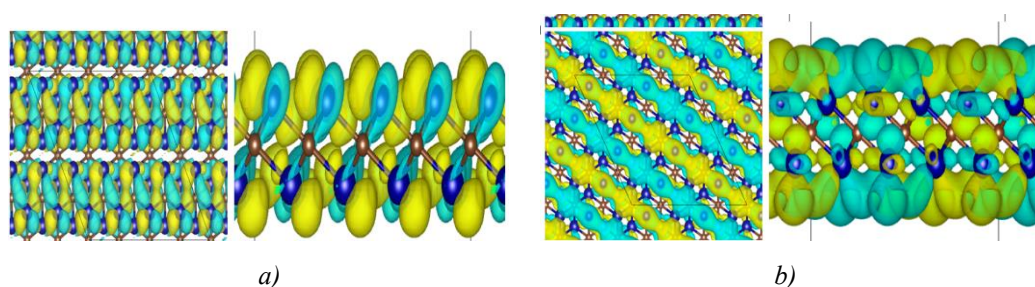


Fig. 3 Top (left) and side (right) views of Cr₂C (a) HOMO structure and (b) LUMO structure. The brown and dark blue balls denote C and Cr atoms, respectively.

The density of state (DOS) of the designed stack is depicted in Fig. 4(a). It is clear from the total DOS (TDOS) that electrons majorly occupy the energy states ranging from -8 ~ 1 eV, meaning that most electrons are below Fermi level as well as a strong interatomic bonding in the Ag/Cr₂C/Pt structures. The projected DOS (PDOS) results also indicate that the *d*-band exhibits higher densities than *s* or *p* bands, which can attributed to the presence of the metal elements (Ag,

Pt and Cr). The energy of the d -band is approximately consistent with the TDOS, showing that metal d electrons mainly contribute to the electron densities, and the chemical activity of the Ag/Cr₂C/Pt device is largely determined by the metal atoms. The calculated device static potential is illustrated in Fig. 4(b). It should be mentioned that the Z-axis fractional coordinates of the topmost layer (i.e., Pt(111)) and the bottommost layer (i.e., Ag(111)), are roughly found to be 0.6 and 1.3 (same as 0.3 due to the periodicity), respectively. There are four negative peaks from 0.5 to 1.5, which are assigned to be Cr₂C, Pt(111), Ag(111) and Cr₂C. The static potential of the region above Pt(111) is slightly higher than that below Ag(111), possibly indicating that cations may be absorbed favorably at the Pt(111) site. Therefore, we considered Ag adsorbed above Pt(111) as the IS. The energy range revealed from the band structures of the considered model (see Fig. 4(c)) varies from -8~1 eV, consistent with the DOS outcome in Fig. 4(a). Note that majority of the energy bands in Fig. 4(c) are found below or at the Fermi level, which is the typical characteristic of the metal system. Only few conduction bands are located above the Fermi level, meaning that electrons are mostly occupied at valence band. The interatomic bonding in Ag/Cr₂C/Pt structure is strong according to results in Fig. 4. Such band gap absence reflected in Figs. 4(a) and 4(c) closely matches the metal-like property implied from Fig. 1(b).

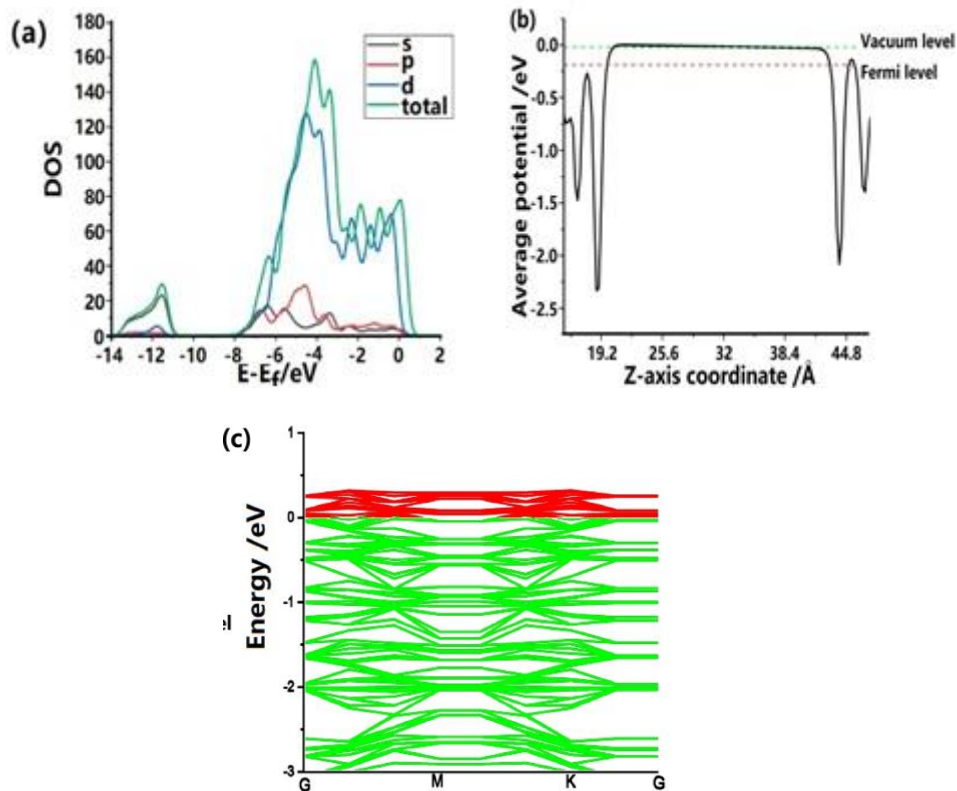


Fig. 4 Electronic structures of Ag/Cr₂C/Pt including (a) total and projected DOS, (b) average static potential along Z-axis, and (c) band structure.

In addition to the electronic structure calculations, it is beneficial to study the contribution of the MXene (e.g., Cr₂C) to the conductive performances of the memristor device whose RS

behavior arises from metal atom diffusion. In this case, the aforementioned DFT model was implemented to predict the electronic characteristics of Ag ion (such as mobility, diffusivity, and electronic conductivity) when migrating through the Ag/Cr₂C/Pt structure. The Ag ion mobility is defined here by [36, 37]:

$$\mu = \left(\frac{\delta^2 \times v_{02} \times q}{6 \times k_B \times T} \right) \times \exp\left(\frac{-E_a}{k_B \times T} \right), \quad (1)$$

where μ is the mobility of Ag ion; v_{02} is the vibration frequency of Ag ion during the transitional state; q is the electronic charge; T is the temperature; k_B is the Boltzmann's constant, and E_a is the activation energy for overcoming the diffusion barrier. δ is the migration distance of Ag ion. The migration direction here was considered as normal to the investigated device and δ was therefore equal to the height of the Ag/Cr₂C/Pt structure in z direction. The calculated mobility was subsequently employed to work out the diffusivity of Ag ion based on:

$$D = \frac{\mu}{q} \times k_B \times T, \quad (2)$$

where D is the diffusivity of the Ag ion migrating inside the designed device. The resulting electrical conductivity during the Ag diffusion was attained based on the Arrhenius equation [38, 33], giving rise to

$$\sigma = A \times \exp\left(\frac{-E_a}{k_B \times T} \right) \quad (3)$$

where σ is the resulting conductivity, and A is the pre-factor, possessed from:

$$A = \frac{k_B \times T}{h} \times \frac{Q^{TS}}{Q^{IS}} \quad (4)$$

where Q^{TS} and Q^{IS} are the partition functions per unit volume for a transition state and a initial state, respectively. Both Q^{TS} and Q^{IS} can be obtained from the calculated vibrational partition function:

$$Q_{vib} = \prod_i \frac{1}{1 - e^{-hc\nu_i/k_B T}} \quad (5)$$

where c and ν_i represent the velocity of light and the vibrational frequency, respectively.

As a result, the electronic characteristics of the Ag ion migration across the Ag/Cr₂C/Pt structure were possessed according to the methods described above integrated with solving eqns (1)-(5). The diffusion barrier E_a was found to be fairly low (~ 0.45 eV). Concerning such a low diffusion barrier, it is expected that Ag ion can readily move along the Z -axis of Ag/Cr₂C/Pt structure at room temperature or even higher temperature. The electronic coefficients can be further described as a function of temperature, and the results are shown in Figure. 5. The diffusivity (Fig. 5(a)) has a range from 10^{-17} to 10^{-10} m²/s with the temperature varying from 223 K to 873 K. The calculated diffusivity seems highly dependent on temperature, and higher temperature can accelerate Ag ion diffusion. Similarly, the results in Fig. 5(b) also suggest that higher mobility is achievable for Ag ion diffusion across the Ag/Cr₂C/Pt structure with

temperatures increasing. The consequent high diffusivity and large mobility of Ag ion when migrating across the Ag/Cr₂C/Pt structure allow for a high electrical conductivity, as results in Fig. 5(c). At room temperature, Ag ion diffusion inside the Ag/Cr₂C/Pt structure exhibits a large conductivity ($\sim 10^2$ S/m), similar to the case with the metal ion diffusing through the liquid. The calculated diffusivity, mobility, and electrical conductivity of the Ag ion diffusion inside the Ag/Cr₂C/Pt at different temperatures were found much higher than those of the Ag/V₂N/Pt structure also calculated from the aforementioned approach. It is also found that the aforementioned electronic properties of Ag ion migrating through the Ag/Cr₂C/Pt stack still give rise to larger values than those of the Ag/Ti₃C₂/Pt stack under the considered temperature. Such superior ion transportation property of the Ag/Cr₂C/Pt is likely to be attributed to its lower diffusion barrier compared with E_a of ~ 0.85 eV and ~ 7.43 eV for the Ti₃N₂ and V₂N stacks, respectively, given that the three aforementioned properties are all correlated with E_a . In addition, such three properties are also linearly correlated with $e^{-1/T}$, resulting in higher values with increasing temperatures. Therefore, it is reasonable to speculate that introducing additional Cr₂C layer into the electrochemical metallization memristor, can remarkably facilitate the Ag ion diffusion and thus form the conductive filament (CF) along the locations of MXene nanostructures. This can strongly suppress the randomness of the CFs and improve the stability and durability of the memristor device. The lower programming voltage is also expected owing to the enhanced conductive characteristic at room temperature.

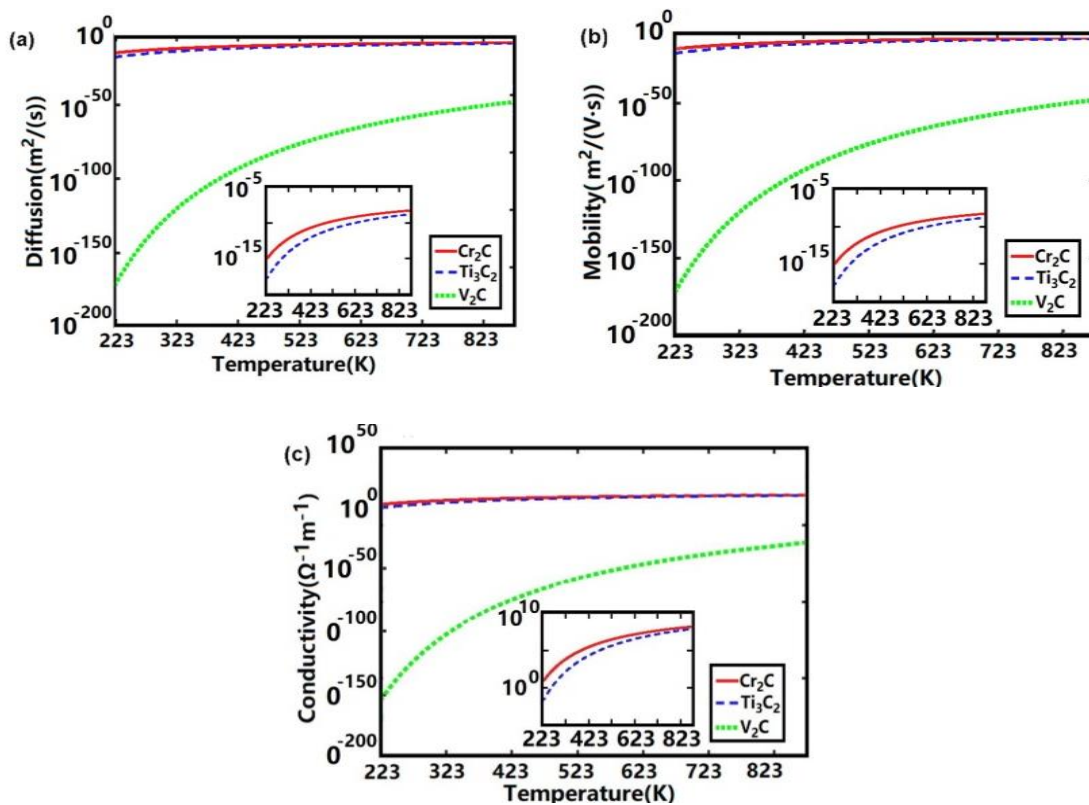


Fig. 5 Electronic coefficients of Ag ion migrating through Ag/MXene/Pt as a function of temperature including (a) diffusivity, (b) mobility, and (c) electrical conductivity for three different MXenes (i.e., Cr₂C, Ti₃N₂, and V₂N). The insets exhibit the electrical characteristics comparison between Cr₂C and Ti₃C₂.

4. Conclusions

In conclusion, the electronic structure and conductive characteristics of the Ag/Cr₂C/Pt device was calculated based on density functional theory. Our simulations clearly revealed that most regions inside the Ag/Cr₂C/Pt stack that exhibited absence of an energy gap were occupied by electrons.

This obviously indicated the metal-like property of the studied structure. Additionally, the investigated Ag/Cr₂C/Pt stack generated lower energy barrier than other conventional MXenes such as Ti₃C₂ and V₂N. This undoubtedly led to higher device electron diffusivity, mobility, and electrical conductivity, thus facilitating the formation of the conductive filaments inside the memristor device. Such device was therefore expected to reduce the randomness of the conductive filament formation and provide great stability and durability.

References

- [1] G. Indiveri, S. C. Liu, *Proc. IEEE* **103**, 1379 (2015).
- [2] C. Rios, M. Stegmaier, P. Hosseini, D. Wang, T. Scherer, C. D. Wright, H. Bhaskaran, W. H. P. Pernice, *Nat. Photonics* **9**, 725 (2015).
- [3] S. Y. Wang, D. W. Zhang, P. Zhou, *Sci. Bull.* **64**, 1056 (2019).
- [4] S. M. Yu, *Proc. IEEE* **106**, 260 (2018).
- [5] S. Desbief, A. Kyndiah, D. Guerin, D. Gentili, M. Murgia, S. Lenfant, F. Alibart, T. Cramer, F. Biscarini, D. Vuillaume, *Org. Electron.* **21**, 47 (2015).
- [6] S. Goswami, S. Goswami, T. Venkatesan, *Appl. Phys. Rev.* **7**, 021303 (2020).
- [7] H. S. Alagoz, M. Davies, Y. Zhong, K. H. Chow, J. Jung, *Solid. State. Commun.* **303**, 113718 (2019).
- [8] F. Gul, *Appl. Nanosci.* **10**, 611 (2019).
- [9] L. Tang, H. Maruyama, T. H. Han, J. C. Nino, Y. H. Chen, D. Zhang, *Appl. Surf. Sci.* **515**, 146015 (2020).
- [10] V. Mikheev, A. Chouprik, Y. Lebedinskii, S. Zarubin, A. M. Markeev, A. V. Zenkevich, D. Negrov, *Nanotechnology* **31**, 215205 (2020).
- [11] X. B. Yan, C. Y. Qin, C. Lu, J. H. Zhao, R. J. Zhao, D. L. Ren, Z. Y. Zhou, H. Wang, J. J. Wang, L. Zhang, X. Y. Li, Y. F. Pei, G. Wang, Q. L. Zhao, K. Y. Wang, Z. A. Xiao, H. Li, *ACS Appl. Mater. Inter.* **11**, 48029 (2019).
- [12] S. Lee, W. R. Zhang, F. Khatkhatay, H. Y. Wang, Q. X. Jia, *Nano. Lett.* **15**, 7362 (2015).
- [13] J. F. Sevic, N. P. Kobayashi, *Appl. Phys. Lett.* **111**, 153107 (2017).
- [14] J. Y. Chen, C. W. Huang, C. H. Chiu, Y. T. Huang, W. W. Wu, *Adv. Mater.* **27**, 5028 (2015).
- [15] Q. Gao, A. P. Huang, Q. Hu, X. J. Zhang, Y. Chi, R. M. Li, Y. H. Ji, X. L. Chen, R. M. Zhao, M. Wang, H. L. Shi, M. Wang, Y. M. Cui, Z. Xiao, P. K. Chu, *ACS. Appl. Mater. Inter.* **11**, 21734 (2019).
- [16] V. A. Volodin, G. N. Kamaev, V. A. Gritsenko, A. A. Gismatulin, A. Chin, M. Vergnat, *Appl. Phys. Lett.* **114**, 233104 (2019).
- [17] A. Schonhals, R. Waser, D. J. Wouters, *Nanotechnology* **28**, 465203 (2017).
- [18] J. Gomez, I. Vourkas, A. Abusleme, R. Rodriguez, J. Martin-Mmartinez, M. Nafria,

- A. Rubio, *Solid-State Electronics*. **165**, 107748 (2020).
- [19] N. He, X. E. Liu, F. Gao, Q. Q. Zhang, M. Zhang, Y. Wang, X. Shen, X. Wan, X. Lian, E. Hu, L. He, J. Xu, Y. Tong, *Mater. Lett.* **266**, 127413 (2020).
- [20] X. Lian, X. Shen, M. Zhang, J. Xu, F. Gao, X. Wan, E. Hu, Y. Guo, J. Zhao, Y. Tong, *Appl. Phys. Lett.* **115**, 063901 (2019).
- [21] M. Naguib, V. N. Mochalin, M. W. Barsoum, Y. Gogotsi, M. Xenos, *Adv. Mater.* **26**, 992 (2014).
- [22] M. R. Lukatskaya, O. Mashtalir, C. E. Ren, Y. Dall'Agnesse, P. Rozier, P. L. Taberna, M. Naguib, P. Simon, M. W. Baarsoum, Y. Gogotsi, *Science* **341**, 1502 (2013).
- [23] J. Pang, R. G. Mendes, A. Bachmatiuk, L. Zhao, H. Ta, T. Gemming, H. Liu, L. Liu, M. H. Rummeli, *Chem. Soc. Rev.* **48**, 72 (2019).
- [24] Y. Q. Wang, X. W. Liu, Y. H. Chen, W. Xu, D. K. Liang, F. Gao, M. C. Zhang, S. Samanta, X. Gong, X. J. Lian, X. Wan, Y. Tong, *Appl. Phys. Express* **12**, 106504 (2019).
- [25] X. B. Yan, K. Y. Wang, J. H. Zhao, Z. Y. Zhou, H. Wang, J. J. Wang, L. Zhang, X. Y. Li, Z. A. Xiao, Q. L. Zhao, Y. F. Pei, G. Wang, C. Y. Qin, J. Z. Lou, Q. Liu, P. A. Zhou, *Small* **15**, 1900107 (2019).
- [26] X. T. Jiang, A. V. Kuklin, A. Baev, Y. Q. Ge, H. Agren, H. Zhang, P. N. Prasad, *Phys. Rep.* **848**, 1 (2020).
- [27] G. Gao, G. Ding, J. Li, K. Yao, M. Wu, M. Qian, *Nanoscale* **8**, 8986 (2016).
- [28] A. S. Ingason, M. Dahiqvist, J. Rosen, *J. J. Phys: Condens. Matter.* **28**, 433003 (2016).
- [29] J. Y. Oh, J. H. Lee, S. W. Han, S. S. Chae, E. J. Bae, Y. H. Kang, W. J. Choi, S. Y. Cho, J. O. Lee, H. K. Baik, T. I. Lee, *Energy Environ Sci.* **9**, 1696 (2016).
- [30] M. Khazaei, M. Arai, T. Sasaki, C. Y. Chung, N. S. Venkataramanan, M. Estili, Y. Sakka, Y. Kawazoe, *Adv Fun Mater.* **23**, 2185 (2013).
- [31] Y. Xie, M. Naguib, V. N. Mochalin, M. W. Barsoum, Y. Gogotsi, X. Yu, K. W. Nam, X. Q. Yang, A. I. Kolesnikov, P. R. C. Kent, *J Am Chem Soc.* **136**, 6385 (2014).
- [32] B. Delley, *J. Chem, Phys.* **92**, 508 (1990).
- [33] B. Delley, B. From Molecules to Solids with The DMol3 Approach, *J. Chem, Phys.* **113**, 7756 (2000).
- [34] A. Yadav, A. Dashora, N. Patel, A. Miotello, M. Press, D. C. Kothari, *Appl. Surf. Sci.* **389**, 88 (2016).
- [35] H. Li, X. Wang, T. Zhang, X. Gong, Q. Sun, H. Pan, Y. Shen, S. Ahmad, M. Wang, *Adv Funct Mater.* **29**, 1903293 (2019).
- [36] B. Li, H. Guo, Y. Wang, W. Zhang, Q. Zhang, L. Chen, X. Fan, W. Zhang, Y. Li, W. Lau, *NPJ. Comp. Mater.* **5**, 16 (2019).
- [37] C. S. His, Y. R. Chen, H. I. Hsiang, *J. Mater. Sci.* **46**, 4695 (2011).
- [38] S. Muneer, J. Scoggin, F. Dirisaglik, L. Adnane, A. Cywar, G. Bakan, K. Cil, C. Lam, H. Silva, A. Gokirmak, *AIP. Adv.* **8**, 065314 (2018).
- [39] R. B. Nuernberg, *Ionics.* **26**, 2405 (2020).